Theoretical and experimental study of dissolution of inhomogeneities formed during spinodal decomposition in polymer mixtures

A. Ziya Akcasu, I. Bahar, B. Erman, Y. Feng, and C. C. Han

Citation: The Journal of Chemical Physics **97**, 5782 (1992); doi: 10.1063/1.463737
View online: http://dx.doi.org/10.1063/1.463737
View Table of Contents: http://scitation.aip.org/content/aip/journal/jcp/97/8?ver=pdfcov
Published by the AIP Publishing

Theoretical and experimental study of dissolution of inhomogeneities formed during spinodal decomposition in polymer mixtures

A. Ziya Akcasu[a)]
Fakultät für physik, Universität Konstanz, D-7750 Konstanz, Germany

I. Bahar and B. Erman
Polymers Research Center and School of Engineering, Bogazici University, Bebek 80815, Istanbul, Turkey

Y. Feng and C. C. Han
Polymers Division, National Institute of Standards and Technology, Gaithersburg, Maryland 20899

(Received 16 March 1992; accepted 8 July 1992)

Dissolution (mixing or melting) of inhomogeneities formed during spinodal decomposition in binary polymer mixtures is studied both experimentally and theoretically. The details of the dissolution experiment with time-resolved light scattering on polystyrene/poly(vinylmethylether) are presented. The theoretical approach differs from that of Langer, Bar-on, and Miller in the way the fluctuations are treated in the nonlinear theory, and in the details of the calculations arising from the chain connectivity (polymer effect). The effect of mode coupling arising from nonlinearity on the relaxation rate is discussed. It is found both experimentally and theoretically that the wave number corresponding to peak intensity decreases in time asymptotically following a $t^{-0.5}$ power law.

I. INTRODUCTION

The kinetics of phase separation in binary mixtures has received a lot of attention in the fields of metallurgy, ceramics, and polymers, and has been an important subject of many theoretical and experimental studies in the past three decades.[1] The motivation for these studies was the possibility of controlling the morphology, especially the possibility of forming cocontinuous materials, through phase separation in the unstable two-phase region. The analysis of the kinetics of phase separation has been centered around the early stage of spinodal decomposition process (SD),[2–7] the intermediate mode-coupling stage,[8] and the late stage scaling analysis.[9–12] Due to the fast decomposition rate and the nonmeanfield nature of liquids, ceramics, and metallurgical systems, the Cahn–Hilliard–Cook[1,2] theory for the early stage spinodal decomposition was never proved unequivocally until binary polymer systems were studied extensively in the last decade.[13–20] The slow decomposition rate and the mean-field nature of the long chain polymer systems are the two major reasons for the success of a quantitative comparison between experiment and theory.

Although the time resolved light scattering studies of polymer systems have enjoyed success in comparing and verifying the linear theory of Cahn–Hilliard–Cook in the early stage of SD and the scaling analysis[21,22] in late stage of SD, a quantitative comparison between experiments and theory is still lacking in the intermediate region. The nonlinear theory of Langer, Bar-on, and Miller[8] is probably the most comprehensive mode-coupling calculation available which is aimed for a solution for the intermediate time region of the SD process. However, this theory is intended for small molecular systems, and does not include the polymeric nature of long chain molecules we will need in our experiment.

We believe that the field has reached a stage where a more complete understanding is needed beyond the mean-field theory and random phase approximation analysis for the structure factor $I(q)$, as well as for the time dependent intensity $I(q,t)$, during transients. [We note that $I(q)$ and $I(q,t)$ will be used in this study instead of $S(q)$ and $S(q,t)$ for the static structure factor because we will only deal with relative scattering intensity, contrary to the absolute scattering intensity, in the light scattering experiment, and also because we want to avoid the confusion with the notation of $S(q,t)$ which is used for the intermediate or dynamic scattering function.] A consistent comparison between experiment and the theory in both demixing (growth) and mixing (dissolution) processes is needed. In this study we present a mode-coupling calculation of the scattering intensity $I(q,t)$ as a function of time t and wave number q, based on a nonlinear stochastic diffusion equation for the order parameter. The theoretical $I(q,t)$ obtained in these calculations can be used, in principle, to describe the results of scattering experiments on binary polymer systems which has been subjected to a step temperature change from miscible one-phase region into the unstable two-phase region, or from the unstable two-phase region (after allowing SD for a short time) back to miscible region. This theoretical calculation is presented in Sec. II. In Sec. III the experimental procedure and measurements are described for a dissolution study by time resolved light scattering on a polystyrene/poly(vinylmethylether) blend. The results will be compared with the theoretical calculation in Sec. IV. Finally, the conclusions will be presented in Sec. V.

[a)]Permanent address: Department of Nuclear Engineering, University of Michigan, Ann Arbor, Michigan 40109.

 0021-9606/92/205782-12$006.00

II. ANALYSIS

A. Description of the theory

The theoretical approach we follow in this paper is essentially the same as the one developed by Langer, Baron, and Miller.[8] There are however differences in the way the fluctuations are included in the nonlinear theory, and in the details of the calculations arising from the chain connectivity (polymer effect) in the case of polymer blends. In addition, the variation of the scattering intensity as a function of time at various wave numbers is studied not only during the spinodal decomposition but also during dissolution. The formalism is also applicable to transients in $I(q,t)$ following step temperature changes within the single phase region.

We consider a melt of two homopolymer species A and B. The volume fractions of monomers at a point $\mathbf{r}$ and time t are denoted by $\phi_A(\mathbf{r},t)$ and $\phi_B(\mathbf{r},t)$. The mixture is assumed to be incompressible so that the local volume fractions satisfy $\phi_A(\mathbf{r},t)+\phi_B(\mathbf{r},t)=1$. When the mixture is in a homogeneous equilibrium state, the volume fractions are uniform and denoted by $\phi_A=\phi_0$ and $\phi_B=1-\phi_0$. The incremental volume fraction of the A component is defined as $\varphi(\mathbf{r},t)\equiv\phi_A(\mathbf{r},t)-\phi_0$. The monomeric volumes v_A and v_B of the species are allowed to be different.

The intensity $I(q,t)$ of the scattering beam in a scattering experiment is related to the Fourier transform of $\varphi(\mathbf{r},t)$

$$I(q,t)=\langle|\varphi_{\mathbf{q}}(t)|^2\rangle, \tag{1}$$

where $\mathbf{q}$ is the momentum transfer vector, and $\varphi_{\mathbf{q}}(t)$ denotes the discrete Fourier transform of $\varphi(\mathbf{r},t)$, i.e.,

$$\varphi_{\mathbf{q}}(t)=\frac{1}{V}\int d^3r\, e^{i\mathbf{q}\cdot\mathbf{r}}\varphi(\mathbf{r},t)$$

in which V is the volume of the system. We note that both $\varphi(\mathbf{r},t)$ and $\varphi_{\mathbf{q}}(t)$ are dimensionless. When the mixture is an equilibrium state, $I(q,t)$ is independent of time, and is given by $I_{eq}(q)=(v_0/V)S(q)$, where v_0 is a reference volume to be specified later, and $S(q)$ is the static structure factor, calculated by de Gennes[23] in the random phase approximation as

$$\frac{1}{S(q)}=\frac{1}{z_AN_A\phi_0f_D(q^2R_{gA}^2)}+\frac{1}{z_BN_B(1-\phi_0)f_D(q_2R_{gB}^2)}-2\chi, \tag{2}$$

in which N_α and $R_{g\alpha}$ denote, respectively, the number of monomers in, and the radius of gyration of, a chain of kind $\alpha=A$, B, and $f_D(x)$ is the usual Debye function

$$f_D(x)=\frac{2}{x^2}(x-1+e^{-x}). \tag{3}$$

In Eq. (2), χ is the Flory interaction parameter, and $z_\alpha=v_\alpha/v_0$ denotes the normalized monomeric volumes relative to the reference volume v_0. It is to be noted that $S(q)$ is proportional to the correlation function $\langle\delta\rho_A(\mathbf{q})\delta\rho_A(-\mathbf{q})\rangle$ of the number density fluctuations $\delta\rho_A(\mathbf{q})$ of species A in the Fourier space, i.e., $S(q)=(v_A^2/v_0V)\langle\delta\rho_A(\mathbf{q})\delta\rho_A(-\mathbf{q})\rangle$.

The intensity $I(q,t)$ becomes time dependent during transients following, for example, a temperature jump from an initial temperature T_{in} in the one-phase region to a final temperature T_f in the spinodal region, leading to spinodal decomposition (demixing), or a temperature drop from T_{in} in the two-phase region to T_f in the one-phase region (reverse quench experiment involving dissolution), or a step temperature change from T_{in} to $T_f<T_{in}$, or vice versa, within the one-phase region.

Following Binder,[4] we start with the free energy excess for a binary mixture of A and B homopolymers

$$\frac{\Delta F}{k_BT}=\int d^3r\frac{1}{v_0}\left\{f[\phi(\mathbf{r})]+\frac{1}{36}\left[\frac{\sigma_A^2}{z_A\phi(\mathbf{r})}+\frac{\sigma_B^2}{z_B[1-\phi(\mathbf{r})]}\right]|\nabla\phi(\mathbf{r})|^2\right\}, \tag{4a}$$

where $\phi(\mathbf{r})=\phi_A(\mathbf{r})$, k_BT is the temperature in energy units, and

$$f(\phi)=\frac{\phi}{z_AN_A}\ln\phi+\frac{(1-\phi)}{z_BN_B}\ln(1-\phi)+\chi\phi(1-\phi). \tag{4b}$$

In Eq. (4a), σ_α denotes the statistical segment lengths of an α chain. When $v_A=v_B=v_0$, and v_0 is set equal to unity, Eqs. (4) reduces to Eqs. (2.1) and (2.2) of Binder[4] (we will use his notations as much as possible to ease comparison), which is valid for slow spatial variations. Equation (4) was previously given, in the case of $v_A\neq v_B$, by Shibayama *et al.*,[24] without the gradient term. The reference volume v_0 was chosen as $v_0=\sqrt{v_Av_B}$. Although the choice of v_0 is arbitrary, this particular one has the advantage that it leads to $z_Az_B=1$, and thus makes the quantity in the curly bracket in Eq. (4a) a function of the ratio of the segmental volumes only. The coefficient of $|\nabla\phi(\mathbf{r})|^2$ in Eq. (4a) is chosen by de Gennes[4] in such a way that the functional differentiation of the above expression of ΔF twice with respect to $\phi_A(\mathbf{r})$ leads to the small-q limit of the static structure factor $S(q)$ in Eq. (2),

$$\frac{1}{S(q)}=2\left\{\chi_s-\chi+\frac{q^2}{36}\left[\frac{\sigma_A^2}{z_A\phi_0}+\frac{\sigma_B^2}{z_B(1-\phi_0)}\right]\right\}, \tag{5a}$$

where χ_s denotes the value of the interaction parameter on the spinodal, i.e.,

$$\chi_s=\frac{1}{2}\left[\frac{1}{z_AN_A\phi_0}+\frac{1}{z_BN_B(1-\Phi_0)}\right], \tag{5b}$$

which is obtained by expanding the Debye function as $f_D(x)=1-x/3$ for small arguments. It is possible to modify the expression of the free energy, as shown by Akcasu and Sanchez,[25] in such a way that it will reproduce the full expression of $S(q)$ in Eq. (2) for all wave numbers. However, this modification will not be needed in the interpretation of the reverse quench experiments under consider-

ation, because in the range of q values involved in the experiment, the Debye function can be expanded as $f_D(x)=1-x/3$.

The functional derivative of ΔF with respect to $\phi_A(\mathbf{r})$ yields the local chemical potential difference (Ref. 4) $\mu(\mathbf{r})$

$$\mu(\mathbf{r})=\frac{k_BT}{v_0}\left\{\frac{1}{z_AN_A}[1+\ln\phi_A]-\frac{1}{z_BN_B}[1+\ln\phi_B]+\chi(1-2\phi_A)-\frac{1}{18}\left[\frac{\sigma_A^2}{z_A\phi_A}+\frac{\sigma_B^2}{z_B\phi_B}\right]\nabla^2\phi_A+\frac{1}{36}\left[\frac{\sigma_A^2}{z_A\phi_A^2}-\frac{\sigma_B^2}{z_B\phi_B^2}\right]|\nabla\phi_A|^2\right\}. \tag{6}$$

When $v_A=v_B=v_0$, and v_0 is set equal to unity, one reproduces Eq. (2.7) of Binder.[4]

The $\varphi_{\mathbf{q}}(t)$ satisfies the following nonlinear stochastic diffusion equation:[6]

$$\frac{\partial\varphi_{\mathbf{q}}(t)}{\partial t}=-q^2V\frac{\Lambda_{\mathbf{q}}}{k_BT}\mu_{\mathbf{q}}(t)+\eta_{\mathbf{q}}(t), \tag{7}$$

where $\Lambda_{\mathbf{q}}$ is the q-dependent Onsager coefficient, which is the discrete Fourier transform of the nonlocal Onsager coefficient $\Lambda(\mathbf{r})$, $\mu_{\mathbf{q}}(t)$ is the discrete Fourier transform of the local chemical potential difference given in Eqs. (6), and $\eta_{\mathbf{q}}(t)$ is the random force accounting for the thermal fluctuations, the statistical properties of which are discussed below. The factor V denoting the volume of the system comes from the discrete Fourier transform of the convolution. In order to obtain an equation for $\varphi_{\mathbf{q}}(t)$, one substitutes $\phi(\mathbf{r},t)=\phi_0+\varphi(\mathbf{r},t)$ in Eqs. (6), expands $\mu(\mathbf{r},t)$ into a power series in power of $\varphi(\mathbf{r},t)$, and then performs discrete Fourier transform. After lengthy but straightforward calculations one obtains

$$\frac{\partial\varphi_{\mathbf{q}}(t)}{\partial t}=-R(q)\left\{\varphi_{\mathbf{q}}(t)+S(q)\sum_{\mathbf{q}_1,\mathbf{q}_2}\Gamma_2(\mathbf{q},\mathbf{q}_1,\mathbf{q}_2)\delta(\mathbf{q},\mathbf{q}_1+\mathbf{q}_2)\varphi_{\mathbf{q}_1}(t)\varphi_{\mathbf{q}_2}(t)+S(q)\sum_{\mathbf{q}_1,\mathbf{q}_2,\mathbf{q}_3}\Gamma_3(\mathbf{q},\mathbf{q}_1,\mathbf{q}_2,\mathbf{q}_3)\delta(\mathbf{q},\mathbf{q}_1+\mathbf{q}_2+\mathbf{q}_3)\varphi_{\mathbf{q}_1}(t)\varphi_{\mathbf{q}_2}(t)\varphi_{\mathbf{q}_3}(t)\right\}+\eta_{\mathbf{q}}(t), \tag{8}$$

where the relaxation frequency $R(q)$ is found as

$$R(q)=q^2\frac{\Lambda(q)}{S(q)} \tag{9}$$

in which $S(q)$ is given in Eq. (2). In the small-q limit, we obtain the more familiar expression of $R(q)$

$$R(q)=2q^2\Lambda(q)\left\{\chi_s-\chi+\frac{q^2}{36}\left[\frac{\sigma_A^2}{z_A\phi_0}+\frac{\sigma_B^2}{z_B(1-\phi_0)}\right]\right\}. \tag{10}$$

We note that this equation includes only the coupling among the concentration modes arising from the nonlinearity of Eq. (7), but does not include the coupling between the modes representing the concentration and the momentum fluctuations. Terms arising from fourth and higher order nonlinearities are neglected. We also note that in Eqs. (9) and (10) we have replaced $\Lambda_{\mathbf{q}}(V/v_0)$ by $\Lambda(q)$ by redefining the Onsager coefficient. The normalization of the latter depends on the normalization used in the definition of the static structure factor $S(q)$. Since the latter is defined in Eq. (2) as a dimensionless quantity, both $\Lambda_{\mathbf{q}}$ and $\Lambda(q)$ have a dimension of cm^2/s. The vertex function $\Gamma_2(\mathbf{q},\mathbf{q}_1,\mathbf{q}_2)$ in Eq. (8) is obtained as follows:

$$\Gamma_2(\mathbf{q},\mathbf{q}_1,\mathbf{q}_2)=U_1-U_2\,\tfrac{1}{2}(q^2+q_1^2+q_2^2), \tag{11a}$$

with

$$U_1=\frac{1}{2}\left[\frac{1}{z_BN_B(1-\phi_0)^2}-\frac{1}{z_AN_A\phi_0^2}\right], \tag{11b}$$

$$U_2=\frac{1}{36}\left[\frac{\sigma_A^2}{z_A\phi_0^2}-\frac{\sigma_B^2}{z_B(1-\phi_0)^2}\right]. \tag{11c}$$

In obtaining Eq. (11a), we symmetrized the second term in Eq. (8) by interchanging $\mathbf{q}_1$ and $\mathbf{q}_2$, adding the resulting equations and dividing by 2. It is to be noted that $\Gamma_2(\mathbf{q},\mathbf{q}_1,\mathbf{q}_2)$ vanishes in the case of a symmetric mixture in which the molecules of the two species are identical to each other so that $N_A=N_B$, $z_A=z_B$, $\sigma_A=\sigma_B$, and $v_A=v_B$, and their volume fractions are equal, i.e., $\phi_0=1/2$. In the present application the mixture is not symmetric, and hence $\Gamma_2(\mathbf{q},\mathbf{q}_1,\mathbf{q}_2)\neq 0$. But it still does not contribute to the final result as a consequence of the Gaussian assumption to be introduced presently [See Eq. (19)].

The vertex function $\Gamma_3(\mathbf{q},\mathbf{q}_1,\mathbf{q}_2,\mathbf{q}_3)$ is calculated as

$$\Gamma_3(\mathbf{q},\mathbf{q}_1,\mathbf{q}_2,\mathbf{q}_3)=Z_1+\frac{Z_2}{6}(q^2+q_1^2+q_2^2+q_3^2), \tag{12a}$$

with

$$Z_1=\frac{1}{3}\left[\frac{1}{z_AN_A\phi_0^3}+\frac{1}{z_BN_B(1-\phi_0)^3}\right], \tag{12b}$$

$$Z_2=\frac{1}{18}\left[\frac{\sigma_A^2}{z_A\phi_0^3}+\frac{\sigma_B^2}{z_B(1-\phi_0)^3}\right]. \tag{12c}$$

In Eq. (8) we terminated the expansion of $\mu(\mathbf{r},t)$ in powers of $\varphi(\mathbf{r},t)$ after the cubic term.

We now come to the specification of the statistical properties of $\eta_q(t)$. It is assumed to be a delta correlated (white) random process with zero mean, and an autocovariance $C(q)$, i.e.,

$$\langle \eta_q(t) \rangle = 0, \tag{13a}$$

$$\langle \eta_q(t)\eta_{-q}(t') \rangle = \delta(t-t')C(q), \tag{13b}$$

$$\langle \eta_q(t)\varphi_{-q}(t) \rangle + \langle \varphi_q(t)\eta_{-q}(t) \rangle = C(q), \tag{13c}$$

$$\langle \eta_q(t)\varphi_{-q}(t') \rangle = 0, \quad t > t'. \tag{13d}$$

The origin of these properties, and the approximations inherent in them have been discussed elsewhere.[26]

The task now is to obtain an equation for the intensity $I(q,t) = \langle |\varphi_q(t)|^2 \rangle$ using the above stochastic nonlinear description of the mixture. For this purpose we multiply Eq. (8) by $\varphi_{-q}(t)$, and its complex conjugate by $\varphi_q(t)$, and add them up. We then take the ensemble average of the resulting equations, and make use of Eq. (13c), obtaining

$$\frac{dI(q,t)}{dt} = -2R(q)\left\{ I(q,t) + S(q)\left[\sum_{\mathbf{q}_1,\mathbf{q}_2} \Gamma_2(\mathbf{q},\mathbf{q}_1,\mathbf{q}_2)\delta(\mathbf{q},\mathbf{q}_1+\mathbf{q}_2)\langle \varphi_{\mathbf{q}_1}(t)\varphi_{\mathbf{q}_2}(t)\varphi_{-\mathbf{q}}(t) \rangle + \sum_{\mathbf{q}_1,\mathbf{q}_2,\mathbf{q}_3} \Gamma_3(\mathbf{q},\mathbf{q}_1,\mathbf{q}_2,\mathbf{q}_3)\delta(\mathbf{q},\mathbf{q}_1 + \mathbf{q}_2+\mathbf{q}_3)\langle \varphi_{\mathbf{q}_1}(t)\varphi_{\mathbf{q}_2}(t)\varphi_{\mathbf{q}_3}(t)\varphi_{-\mathbf{q}}(t) \rangle \right] \right\} + C(q). \tag{14}$$

In the linear theory, Eq. (14) is approximated by

$$\frac{dI(q,t)}{dt} = -2R(q)I(q,t) + C(q),$$

with a solution

$$I(q,t) = I_{\text{in}}(q,t)e^{-2R(q)t} + I_{\text{eq}}(q)[1 - e^{-2R(q)t}], \tag{15}$$

which is the celebrated Cahn–Hilliard–Cook form (CHC) for polymer mixtures.[2,3] In obtaining Eq. (15), we have eliminated $C(q)$ requiring that $I(q,t) \to I_{\text{eq}}(q)$ as $t \to \infty$. This leads to

$$C(q) = 2R(q)I_{\text{eq}}(q) \tag{16a}$$

$$= 2q^2\Lambda_q, \tag{16b}$$

which is Einstein's relation,[27] or one form of the fluctuation–dissipation theorem.

We mention in passing that in a recent publication[26] we provided a non-Markovian extension of the CHC theory in matrix form using a microscopic approach based on the Zwanzig–Mori projection operator technique, and investigated the nature of approximations in it. In the special case of scattering from one component, we obtained

$$I(q,t) = I_{\text{in}}(q)S^2(q,t) + I_{\infty}(q)[1 - S^2(q,t)], \tag{17}$$

where $S(q,t)$ is the normalized [$S((q,0) = 1)$ dynamic or intermediate] scattering function in the final equilibrium state, i.e.,

$$S(q,t) = \frac{\langle \varphi_q(t)\varphi_q(0)^* \rangle}{\langle |\varphi_q|^2 \rangle}. \tag{18}$$

We note that $S(q,t)$ does not have to be exponential, as in the conventional CHC theory. The microscopic derivation does not contain phenomenological quantities such as the Onsager coefficient $\Lambda(q)$, nor does it require the incompressibility assumption.

In the nonlinear theory, one has to introduce approximations to express the third and fourth order correlation functions in Eq. (14), in terms of $I(q,t)$. If we assume, following Langer,[8,28] that $\varphi_q(t)$ for different values of $\mathbf{q}$ are Gaussian random variables with zero mean, then we have

$$\langle \varphi_{\mathbf{q}_1}(t)\varphi_{\mathbf{q}_2}(t)\varphi_{-\mathbf{q}}(t) \rangle = 0, \tag{19}$$

$$\langle \varphi_{\mathbf{q}_1}(t)\varphi_{\mathbf{q}_2}(t)\varphi_{\mathbf{q}_3}(t)\varphi_{-\mathbf{q}}(t) \rangle = \langle \varphi_{\mathbf{q}_1}(t)\varphi_{\mathbf{q}_2}(t) \rangle \langle \varphi_{\mathbf{q}_3}(t)\varphi_{-\mathbf{q}}(t) \rangle + \langle \varphi_{\mathbf{q}_1}(t)\varphi_{\mathbf{q}_3}(t) \rangle \langle \varphi_{\mathbf{q}_2}(t)\varphi_{-\mathbf{q}}(t) \rangle + \langle \varphi_{\mathbf{q}_1}(t)\varphi_{-\mathbf{q}}(t) \rangle \langle \varphi_{\mathbf{q}_2}(t)\varphi_{\mathbf{q}_3}(t) \rangle.$$

Using

$$\langle \varphi_{\mathbf{q}_i}(t)\varphi_{\mathbf{q}_j}(t) \rangle = \langle \varphi_{\mathbf{q}_i}(t)\varphi_{-\mathbf{q}_i}(t) \rangle \delta(\mathbf{q}_i + \mathbf{q}_j),$$

we find

$$\langle \varphi_{\mathbf{q}_1}(t)\varphi_{\mathbf{q}_2}(t)\varphi_{\mathbf{q}_3}(t)\varphi_{-\mathbf{q}}(t) \rangle = 3I(q,t)I(q_1,t)\delta(\mathbf{q}_1 - \mathbf{q})\delta(\mathbf{q}_2 + \mathbf{q}_3). \tag{20}$$

Substitution of Eqs. (19) and (20) into Eq. (14) yields

$$\frac{dI(q,t)}{dt} = -2R(q)I(q,t)[1 + Z(q,t)] + C(q), \tag{21}$$

where

$$Z(q,t) = \sum_{q'} \gamma(q,q')I(q',t). \tag{22}$$

In Eq. (22) we have introduced

$$\gamma(q,q') = 3\Gamma_3(\mathbf{q},-\mathbf{q},\mathbf{q}',-\mathbf{q}')S(q), \tag{23a}$$

where $\Gamma_3(\mathbf{q},-\mathbf{q},\mathbf{q}',-\mathbf{q}')$ is to be obtained from Eqs. (12) with obvious change in the arguments, and $S(q)$ is given in Eq. 2. In the small limit, for example, one has

$$\gamma(q,q')=\frac{3}{2}\frac{Z_1+(Z_2/3)(q^2+q'^2)}{\chi_s-\chi+(q^2/36)[\sigma_A^2/z_A\phi_0+\sigma_B^2/z_B(1-\phi_0)]}, \tag{23b}$$

where Z_1 and Z_2 are defined in Eqs. (12b) and (12c).

The assumption that the $\varphi_{\mathbf{q}}(t)$ for different values of $\mathbf{q}$ are Gaussian random variables with zero mean, is equivalent to treating $\varphi(\mathbf{r},t)$ at different values of $\mathbf{r}$ as a multivariate Gaussian process with zero mean so that fourth order correlation functions in the configuration space can also be factorized. For example,

$$\langle\varphi^3(\mathbf{r},t)\varphi(\mathbf{r}',t)\rangle=3\langle\varphi^2(\mathbf{r},t)\rangle I(\mathbf{r}-\mathbf{r}',t), \tag{24a}$$

which was used by Langer.[28] If $\gamma(q,q')$ in Eq. (22) were independent of q' and equal to $\gamma(q)$, then the function $Z(q,t)$ could be assessed as the average variance of the local volume fraction fluctuations as

$$Z(q,t)=\gamma(q)\frac{1}{V}\int_V d\mathbf{r}\langle\varphi(\mathbf{r},t)^2\rangle, \tag{24b}$$

which follows from the Parseval relation relating the Fourier pairs. In the small particle limit in which σ_A and $\sigma_B\to 0$, $Z(q,t)$ would be independent of q, and be proportional to $A(t)$ in the Langer theory. Equation (22) shows that the function $Z(q,t)$ represents the effect of mode coupling on the time evolution of $I(q,t)$. Indeed, Eq. (21) can be solved in terms of $Z(q,t)$ as

$$I(q,t)=I_{\text{in}}(q)e^{-2R(q)[t+\int_0^t dt' Z(q,t')]}+C(q)\int_0^t du\, e^{-2R(q)[u+\int_0^u dt' Z(q,t-t')]}. \tag{25}$$

The magnitude of the noise source $C(q)$ is determined from the requirement that $I(q,t\to\infty)=I_{\text{eq}}(q)$

$$C(q)=2R(q)I_{\text{eq}}(q)[1+Z_{\text{eq}}(q)], \tag{26a}$$

where

$$Z_{\text{eq}}(q)=\sum_{\mathbf{q}'}\gamma(q,q')I_{\text{eq}}(q'). \tag{26b}$$

Equation (26a) is a statement of the fluctuation–dissipation theorem, which determines the magnitude $C(q)$ of the random force in the Langevin equation in terms of the equilibrium static structure factor $I_{\text{eq}}(q)$. The latter is to be calculated in principle using the equilibrium distribution function $P_{\text{eq}}(\{\phi\})\propto\exp(-\beta\Delta F)$. However, as pointed out by Fredrickson,[5] the expression of $I_{\text{eq}}(q)$ in Eq. (2), which is obtained with the mean-field theory, provides an excellent approximation to the equilibrium structure factor, even relatively close ($|1-\chi/\chi_s|\geqslant 0.01$) to the critical point. With this approximation, Eq. (26a) yields

$$C(q)=2q^2\Lambda_{\mathbf{q}}[1+Z_{\text{eq}}(q)]. \tag{26c}$$

In the linear theory $C(q)$ was given by $2R(q)I_{\text{eq}}(q)$ or by $2q^2\Lambda_{\mathbf{q}}$ [cf. Eq. (16)]. We find that in the nonlinear theory the magnitude of the Langevin random force is renormalized by the additional factor $[1+Z_{\text{eq}}(q)]$. The normalization of $C(q)$ implies in turn a renormalization of the free energy functional. The procedure followed here differs from that used by Fredrickson,[5] who also approximates $I_{\text{eq}}(q)$ by its mean-field expression, but retains, in Eq. (26a), the expression of $C(q)$ in the linear theory and renormalizes the location of the critical point to satisfy the resulting equation. It seems that both procedures are justified within the approximations introduced in the derivation of Eq. (21) and in the equilibrium static structure factor. The choice in Eq. (26c) proves to be convenient in the numerical solution of Eq. (21), because it does not require readjustment of the interaction parameter at each q, and still insures that the solution of Eq. (21) approaches the static structure factor in the random phase approximation as $t\to\infty$.

Equation 25 shows that the linear CHC form is recaptured when $Z(q,t)$ is set equal to zero. A comparison with the linear theory suggests that the product

$$\Omega(q,t)=R(q)[1+Z(q,t)] \tag{27}$$

can be interpreted as a time-dependent instantaneous relaxation frequency. It is therefore interesting to investigate the q and time dependence of $Z(q,t)$, and hence $\Omega(q,t)$.

B. Computational details

We first present the numerical solution of Eq. (21) for $I(q,t)$ by writing Eq. (21) in a slightly different form as

$$\bar{I}(q,t+\Delta t)=\bar{I}(q,t)+\Delta t\{-2R(q)\bar{I}(q,t)[1+Z(q,t)]+\bar{C}(q)\}, \tag{28}$$

where we have renormalized the intensity and the power spectral density of the random noise as $\bar{I}(q,t)=(V/v_0)I(q,t)$ and $\bar{C}(q)=2R(q)\bar{I}_{\text{eq}}(q)[1+Z_{\text{eq}}(q)]$, respectively. The reason for this change in notation will be apparent shortly. It is clear that $\bar{I}_{\text{eq}}(q)$ is equal to the static structure factor $S(q)$ given in Eq. (2). In Eq. (10), the relaxation frequency $R(q)$ as well as the static structure factor $\bar{I}_{\text{eq}}(q)$ are to be calculated at the final temperature T_{f} in the one-phase region in a reverse quench experiment, or in the case of a step temperature change in one phase. In other words, the Onsager coefficient $\Lambda(q)$ and the Flory interaction parameter χ appearing in the expressions of $R(q)$ and $\bar{I}_{\text{eq}}(q)$ are to be evaluated at T_{f}. In the case of a temperature jump into the spinodal region, the final state at T_{f} is not accessible during the demixing process, and hence $\bar{C}(q)$ is calculated using $\bar{I}_{\text{eq}}(q)$ at the initial temperature assuming that the magnitude of the noise term is not altered significantly during the small temperature changes. We shall elaborate this point further in an accompanying paper involving spinodal decomposition.

The calculation of $Z_{\text{eq}}(q)$ using Eq. (26b) requires some care. First one must convert the discrete summation on $\mathbf{q}'$ to an integration as

$$Z_{eq}(q)=\frac{V}{(2\pi)^3}\int dq'\,\gamma(q,q')I_{eq}(q')$$

$$=\frac{V}{2\pi^2}\int_0^{q_{cut}} dq'\,q'^2\gamma(q,q')I_{eq}(q')$$

$$=\frac{v_0}{2\pi^2}\int_0^{q_{cut}} dq'\,q'^2\gamma(q,q')\bar{I}_{eq}(q'). \tag{29}$$

The upper cutoff wave number q_{cut} is introduced because the integral in Eq. (29), in which $\bar{I}_{eq}(q)$ is substituted from Eq. (2), is divergent. The physical implication is that only the modes with wave numbers between zero and q_{cut} are coupled to each other. It is therefore reasonable to choose[8] q_{cut} smaller or equal to the inverse correlation length $q_c=\xi^{-1}$. The latter is defined by expressing $S(q)$ in Eq. (5a) as $S(q)=S(0)/(1+q^2\xi^2)$

$$\frac{1}{q_c}=\xi=\left\{\frac{1}{36(\chi_s-\chi)}\left[\frac{\sigma_A^2}{z_A\phi_0}+\frac{\sigma_B^2}{z_B(1-\phi_0)}\right]\right\}^{1/2}. \tag{30}$$

In evaluating the integral in Eq. (29) with $q_{cut}\leqslant q_c$, we can use the small-q limits of $\bar{I}_{eq}(q)=S(q)$ given in Eq. (5a), and of $\gamma(q,q')$ given in Eq. (23b). The result can be obtained analytically as follows:

$$Z_{eq}(q)=\frac{3}{8\pi^2}\frac{v_0q_c^3}{(\chi_s-\chi)^2}\frac{1}{1+q^2\xi^2}\left\{(\alpha-\tan^{-1}\alpha)\left(Z_1+\frac{Z_2q^2}{3}\right)+\left(\tan^{-1}\alpha+\frac{\alpha^3}{3}-\alpha\right)\frac{Z_2q_c^2}{3}\right\}, \tag{31}$$

where Z_1 and Z_2 are given in Eqs. (12). In Eq. (31) we have introduced $\alpha=q_{cut}/q_c$, as a measure of the range of mode coupling. We treat α as an adjustable parameter in the theory, with values $\alpha\leqslant 1$.

The $Z(q,t)$ in Eq. (28) is to to be calculated at each discrete time using

$$Z(q,t)=\frac{v_0}{2\pi^2}\int_0^{q_{cut}} dq'\,q'^2\gamma(q,q')\bar{I}(q',t) \tag{32a}$$

or substituting $\gamma(q,q')$ from Eq. (23b)

$$Z(q,t)=\frac{3}{4\pi^2}\frac{v_0q_c^3}{(\chi_s-\chi)}\frac{1}{1+q^2\xi^2}\left\{\int_0^{\alpha} dx\,x^2\left[Z_1+\frac{Z_2}{3}(q^2+x^2q_c^2)\right]\bar{I}(xq_c,t)\right\}, \tag{32b}$$

where we have defined $x=q'/q_c$.

Equation (28) can now be solved numerically starting from a given initial intensity $\bar{I}_{in}(q)$, calculating $Z(q,0)$ from Eq. (32), and finding $\bar{I}(q,\Delta t)$, and so on. Since the intensities in a scattering experiment are measured in arbitrary units, one has to introduce a scaling factor to convert the experimental values to the absolute intensities as $\bar{I}_{in}(q)=A_0I_{in}^{exp}(q)$, where A_0 is to be treated as an adjustable parameter. The number α in Eqs. (31) and (32) is also to be considered an adjustable parameter in the vicinity of $\alpha=1$, as mentioned earlier.

III. EXPERIMENT

In this paper we will only make a detailed comparison between the above theoretical calculations and the dissolution experiments performed with polystyrene/poly(vinylmethylether) (PS/PVME) near its critical composition. Experimental results for this system for early stage SD (Ref. 20) and reverse quench within the one-phase region[29] (decay of concentration fluctuations) have been published elsewhere before. A nonlinear description of these two cases will be presented in a future publication.

A. Samples

Blends of 80 wt % PVME and 20 wt % PS [contained 0.05 wt % 4,4′-thiobis (6,tert-butyl-*m*-cresol) as the antioxidant] were used in this study. The polystyrene is a TSK[30] standard from Tosoh Corp. which has a weight-average molecular weight $M_w=1.86\times10^5$ and a molecular weight distribution index $M_w/M_n=1.07$. The poly(vinylmethylether) was cationically polymerized and fractionated, which has a weight-average molecular weight $M_w=1.71\times10^5$ and a molecular weight distribution index $M_w/M_n=1.42$ determined by size exclusion chromatography.[31]

The sample films were prepared by casting from toluene solution (about 10% total polymer concentration) on quartz window plates. The film was dried in vacuum at room temperature for two days, and at 70 °C for two more days. Then it is covered by another quartz plate with a metal spacer of 0.1 mm thick to maintain specimen thickness.

As determined in a previous study[29] this blend has a spinodal temperature $T_s=115.2$ °C, and is at the critical composition.[20,21]

B. Measurement

The reverse quench experiment in this study were carried out on a time-resolved static light scattering instrument. The detailed instrumentation has been described elsewhere.[20,29,32] The temperature in the preheating block was set to a value in the immiscible region of the blend, at which the blend developed a certain structure corresponding to different stage of spinodal decomposition. The temperature in the main block was controlled at a desired experimental temperature which is in the miscible region of the blend. The reverse quench (dissolution) experiment was carried out by quickly transferring samples from the preheating block to the main block. The initial time of the experiment is chosen to be at the end of 1 min after transferring the sample into the main block, during which time the sample is believed to have reached the final equilibrium temperature. The angular dependence of the scattering intensity at various times after this reverse quench are then recorded.

TABLE I. Characterization of the mixture.

Monomeric mass numbers:	$m_A=104$	$m_B=58$
Bulk densities (g/cm^3):	$\rho_A=1.04$	$\rho_B=1.04$
Monomeric volumes (cm^3):	$v_A=1.66\times10^{-22}$	$v_B=0.93\times10^{-22}$
Reference monomeric volume (cm^3):	$v_0=\sqrt{v_A v_B}=1.24\times10^{-22}$	
Relative monomeric volumes:	$z_A=v_A/v_0=1.34$	$z_B=0.75$
Volume fractions:	$\phi_A=0.2$	$\phi_B=0.8$
Spinodal temperature:	$T_s=115.2$ °C	
Interaction parameter at T_s:	$\chi_s=1.328\times10^{-3}$	

IV. COMPARISON OF THEORETICAL AND EXPERIMENTAL RESULTS AND DISCUSSIONS

A. Calculation of the input parameters

The relevant properties of the mixture are given in Table I. The labels A and B in the table refer to the PS and PVME, respectively. The monomeric volumes are calculated using $v_\alpha=m_\alpha/\rho_\alpha N_{av}$ where N_{av} is the Avagadro's number. The interaction parameter χ_s at the spinodal temperature T_s is calculated using Eq. (5b). Interaction parameters at different temperatures are calculated using[20,29]

$$\frac{2}{v_0}[\chi_s-\chi(T)]=2.18\times10^3\left(\frac{1}{T}-\frac{1}{T_s}\right)\frac{1}{k_BT},$$

where $k_B=1.38\times10^{-23}$ J/K. At the initial and final temperatures in the reverse quench experiment we find

$$\chi(119\,^\circ\text{C})=1.95\times10^{-3}=1.47\chi_s,$$

$$\chi(110\,^\circ\text{C})=0.435\times10^{-3}=0.33\chi_s.$$

The physical properties of the chains are summarized in Table II. The σ_α in the table denote the segment lengths that yield the measured radius of gyrations with the actual number of monomers N_α in $R_{g\alpha}^2=N_\alpha\sigma_\alpha^2/6$, rather than the statistical segment lengths.[33]

B. Onsager coefficient

The Onsager coefficient Λ, and the interdiffusion coefficient D_{int} are to be evaluated at the final temperature following the temperature drop, which is $T_f=110$ °C in the experiment being analyzed. In an independent experiment involving a temperature drop from 117 °C to 110 °C, D_{int} was inferred from the small-q limit of the relaxation frequency $R(q)$ (Ref. 29) as

$$D_{int}=2.1\times10^{-13}\ \text{cm}^2/\text{s}.$$

Since the interdiffusion coefficient is defined as

$$D_{int}=\lim_{q\to0}\frac{R(q)}{q^2},$$

we obtain

$$D_{int}=2\Lambda[\chi_s-\chi(110\,^\circ\text{C})].$$

With the data given above, one finds

$$\Lambda(110\,^\circ\text{C})=1.21\times10^{-10}\ \text{cm}^2/\text{s}.$$

It is to be noted however that the above value represents an upper bound for Λ, inasmuch as the interdiffusion coefficient should be proportional to the time dependent relaxation frequency $\Omega(q,t)=R(q)[1+Z(q,t)]$.

At other temperatures, $\Lambda(T)$ is calculated using[29]

$$\Lambda(T)=\Lambda(T_1)\exp\left[-2\times10^4\left(\frac{1}{T}-\frac{1}{T_1}\right)\right],$$

where T is in K.

TABLE II. Properties of the chains.

Molecular weights:	$M_A=1.86\times10^5$	$M_B=1.71\times10^5$
Number of monomers:	$N_A=1800$	$N_B=2950$
Radius of gyrations (Å):	$R_{gA}=117$	$R_{gB}=150$
Segment lengths (Å):	$\sigma_A=6.8$	$\sigma_B=6.8$

C. Interpretation of data

In this section, we analyze the intensity data on PVME–PS mixture following a temperature drop from 119 °C in biphasic region to 110 °C in one-phase region, by solving the difference Eq. (28) for discrete values of q with the parameters determined above. In these calculations the cutoff wave number q_c is chosen as the inverse correlation length so that $\alpha=1$. Experimentally reported intensities $I_{expt}(q,t)$, which are in arbitrary units, are converted into absolute values $I(q,t)$ by rescaling them with a conversion factor A_0 according to $I(q,t)=A_0I_{expt}(q,t)$. The value $A_0=1.5$ is adopted, as deduced from the best fit between theory and experiment. Initial intensities $I(q,0)$ which are needed to initiate the computation are obtained by smoothing the rescaled experimental values. $I(q,0)$ values are used in Eq. (32b) to calculate $Z(q,0)$, which is also needed for determining $I(q,t)$ at subsequent times, following Eq. (28). Reasonable agreement between theory and experiment in the time range $120\leqslant t\leqslant1440$ s is obtained if the Onsager coefficient is decreased approximately by half from the above calculated value $\Lambda(110\,^\circ\text{C})=1.21\times10^{-10}$ to 0.605×10^{-10} cm^2/s. Likewise an increase in the initial intensities by 10% is found to lead to better agreement with experiment. The need for those readjustments can be partially attributed to the uncertainty in the initialization time of the dissolution process, after the implementation of the temperature drop to 110 °C. Indeed, the first set of intensities which are experimentally presented as the $I(q,0)$ data, are taken 60 s after the implementation of the step temperature change, in order to permit an equilibration of the system with the main block at 110 °C. Dissolution may have started somewhat earlier than 60 s. Also, noting that the original value for the Onsager coefficient is inferred from the linear analysis of an independent experiment involving a temperature drop from 117 °C to 110 °C, a smaller value for $\Lambda(110\,^\circ\text{C})$ presently adopted may seem reasonable.

The theoretical and experimental results are compared in Figs. 1 and 2 for the dissolution time ranges of

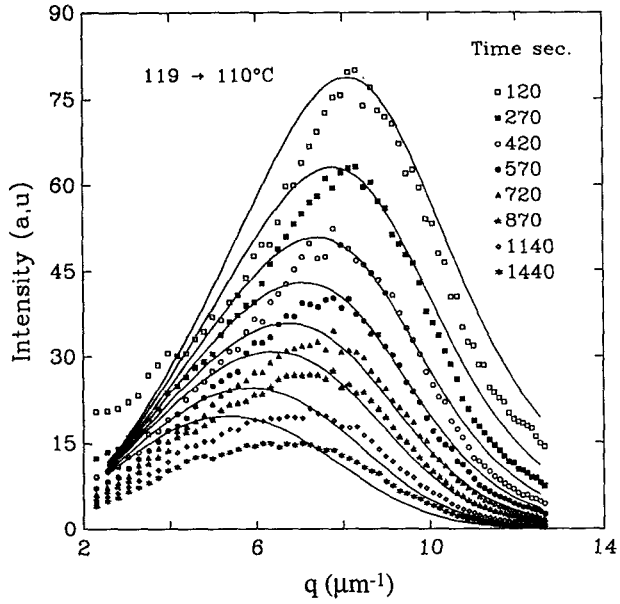

FIG. 1. Variation of the intensity $I(q,t)$ with wave number for various dissolution times following a temperature drop from 119 °C (biphasic region) to 110 °C (single phase region). The points represent data from the reverse quench experiment in the range $120 \leqslant t \leqslant 1440$ s, as indicated. The curves are calculated according to the present theory by connecting intensities $I(q,t)$ computed at discrete q values. The uppermost curve represent $I(q,0)$.

$120 \leqslant t \leqslant 1440$ s and $1580 \leqslant t \leqslant 2700$ s, respectively. In the figures the points represent the experimental results at various times, as indicated, and the corresponding curves are obtained from the theory. In general, the qualitative features of the data are satisfactorily reproduced by the theory. The quantitative agreement in Fig. 1 is also considered satisfactory, in view of the uncertainties both in the experiment and in the numerical values of the parameters used in the theoretical analysis. The agreement becomes progressively poorer at longer times, as may be observed from Fig. 2, which displays the results for $t \geqslant 1560$ s. We have no explanation for this discrepancy.

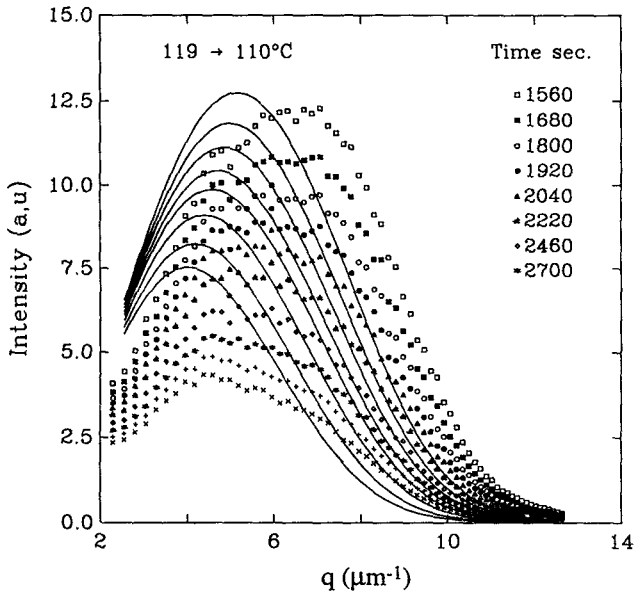

FIG. 2. Same as in Fig. 1 for the time range $1560 \leqslant t \leqslant 2700$ s.

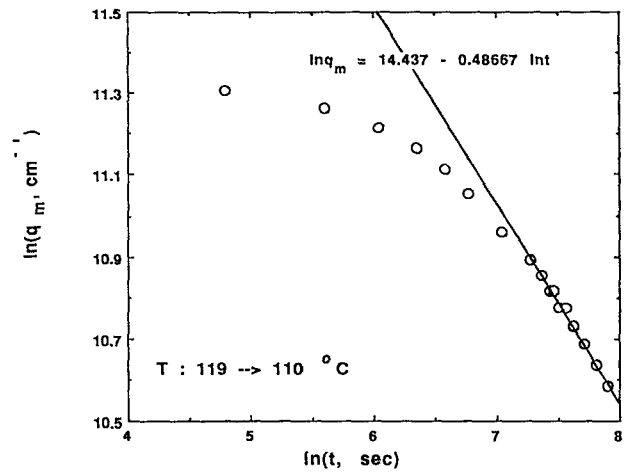

FIG. 3. Variation of the wave number $q_m(t)$, where the intensity is maximum, with time in a reverse quench experiment (theoretical).

A more universal feature of the intensity data is the variation with time of $q_m(t)$, which is the wave number where the intensity attains its maximum at a fixed t. Figure 3 shows that $q_m(t)$ obeys a power law at large times, and decreases as $t^{-1/2}$ with time in the time interval where the first term is dominant (dissolution stage) in Eq. (25). This behavior can be explained theoretically by differentiating the latter with respect to q (more conveniently with respect to q^2) and equating the result to zero. The result is

$$\left.\frac{d \ln I_{\text{in}}(q)}{dq^2}\right|_{q=q_m(t)} = 2\frac{d}{dq^2}\left\{R(q)\left[t + \int_0^t dt'\, Z(q,t')\right]\right\}_{q=q_m(t)}.$$

For large times, the right hand side behaves as $\{tR(q)[1+Z_{\text{eq}}(q)]\}$. Since $Z_{\text{eq}}(q)$ is nearly independent of q [see Fig. 4(a), and use $Z_{\text{eq}}(q)=Z(q,t\to\infty)$], we can also ignore its derivative [also, the latter is multiplied by $q_m(t)^2$, and $q_m(t)\to 0$ as $t\to\infty$], and obtain

$$\left.\frac{d \ln I_{\text{in}}(q)}{dq^2}\right|_{q=q_m(t)} = 2t[1+Z_{\text{eq}}(0)]\left.\frac{dR(q)}{dq^2}\right|_{q=q_m(t)}, \tag{33}$$

where $R(q)$ given in Eq. (10), and $Z_{\text{eq}}(q)$ in Eq. (31). The derivative $R(q)$ is obtained from Eq. (10) in the small-(q) limit as $2\Lambda(\chi_s-\chi)$, which is the D_{int}. Hence,

$$\left.\frac{d \ln I_{\text{in}}(q)}{dq^2}\right|_{q=q_m(t)} = 2tD_{\text{int}}[1+Z_{\text{eq}}(0)], \tag{34a}$$

where $Z_{\text{eq}}(0)$ follows from Eq. (31) with $\alpha=1$ as

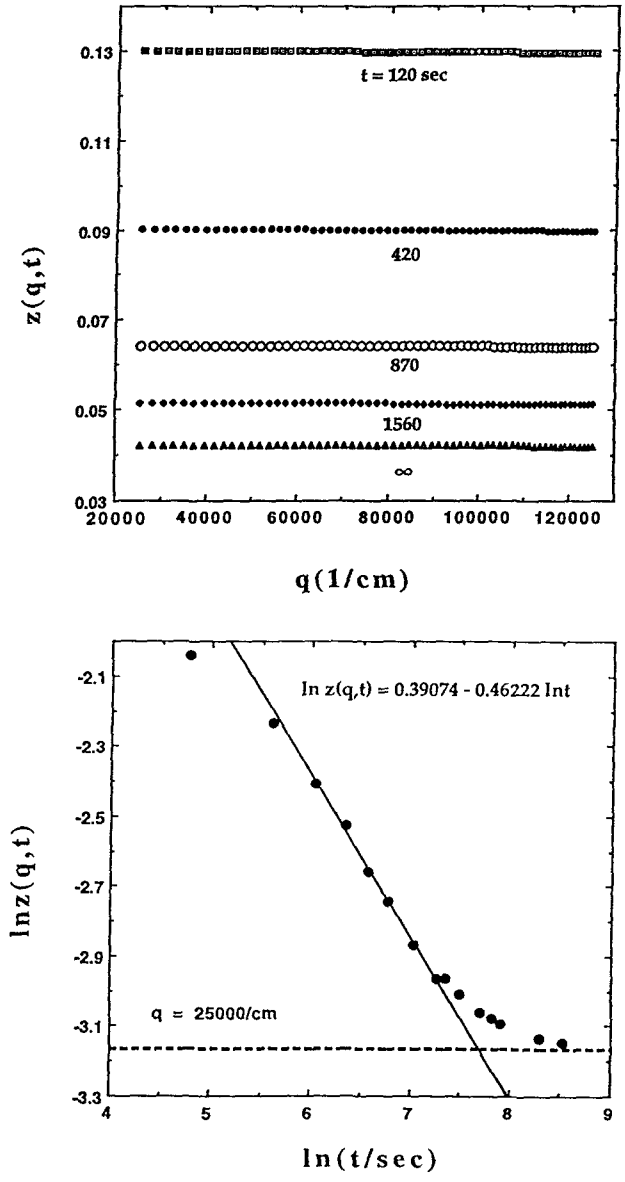

FIG. 4. Variation of $Z(q,t)$ in the expression of the instantaneous relaxation frequency $\Omega(q,t)=R(q)[1+Z(q,t)]$ with wave number and time.

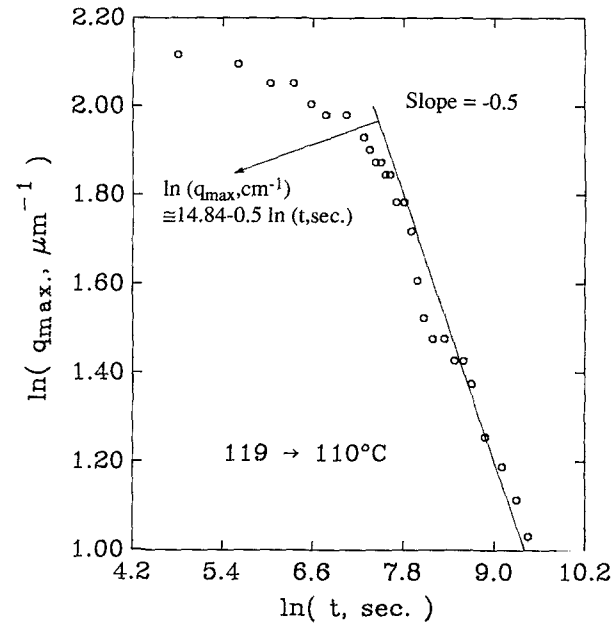

FIG. 5. Variation of the wave number $q_m(t)$, where the intensity is maximum, with time in a reverse quench experiment from 119 °C to 110 °C. The circles denote the experimental values.

$$Z_{eq}(0)=\frac{3}{8\pi^2}\frac{v_0 q_c^3}{(\chi_s-\chi)^2}\left|\left(1-\frac{\pi}{4}\right)Z_1+\left(\frac{\pi}{4}-\frac{2}{3}\right)\frac{Z_2 q_c^2}{3}\right| \tag{34b}$$

and is small as compared to unity unless χ is very close χ_s. The crucial quantity in Eq. (34a) that determines the asymptotic behavior of $q_m(t)$ is the variation of $\ln I_{in}(q)$ with q. This depends on the preparation of the initial state. In the reverse quench experiments, the latter is prepared by spinodal decomposition starting from an equilibrium state, and by allowing the system to phase separate sufficiently so that the late stage is reached. In this stage of spinodal decomposition, the intensity obeys dynamic scaling[11,34] such that its q dependence at a time t, in particular at $t=t_w$, at which the reversed quench is initiated, can be represented $I_{in}(q)\sim q_m(t_w)^{-3}x^2/(2+x^6)$ where $x=q/q_m(t_w)$.

Therefore, $d\ln I_{in}(q)/d\,q^2=q^{-2}$ in the limit of $q_m(t)\to 0$. Substitution of this result into Eq. (34a) yields

$$q_m(t)^2\to\frac{1}{2[1+Z_{eq}(0)]D_{int}t}. \tag{35}$$

It is noted that this power-law behavior depends on the q dependence of the initial intensity in the small-q limit, and thus on its preparation. Had the latter been prepared in a different process from spinodal decomposition, a different power law would be conceivable. Using $D_{in}(110\,°C)=1.05\times10^{-13}$ cm^2/s, which was used in the numerical calculations, and $Z_{eq}(0)=0.042$ [$Z(0,t\to0$ in Fig. 4] in Eq. (35) we find

$$\ln q_m(t)=14.57-0.5\ln t. \tag{36}$$

This asymptotic behavior is consistent with that obtained numerically in Fig. 3 as $\ln q_m(t)=14.437-0.487\ln t$. Small discrepancies in the intercept and the slope can be attributed to the fact that the asymptotic region has not quite been reached in the numerical integration. The agreement with the experimental result $\ln q_m(t)=14.84-0.5\ln t$ shown in Fig. 5 is also very satisfactory.

The Eq. (35) suggests a procedure to extract the interdiffusion coefficient from the data representing $q_m(t)$ vs t. Since the intercept is equal to $0.5\times\ln\{2[1+Z_{eq}(0)]D_{in}\}^{-1}$, we can infer D_{in} from it. However, this procedure is not accurate because of the logarithmic relationship between the intercept and $[1+Z_{eq}(0)]D_{in}$. As an illustration, we find $D_{in}=0.62\times10^{-13}$ cm^2/s with the experimental value of 14.84. This value, is about 1/3.4 of the diffusion coefficient obtained earlier,[29] and 1/1.7 of that which was used in the numerical integration of Eq. (21). Similarly we extract the interdiffusion coefficient at 114 °C

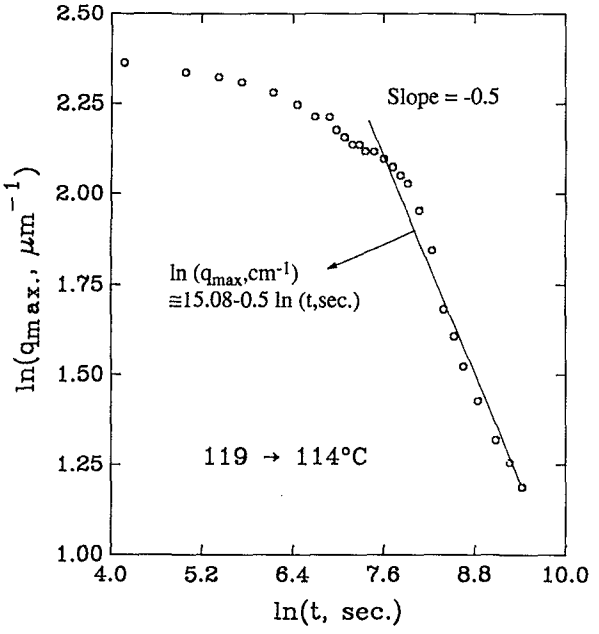

FIG. 6. Variation of the wave number $q_m(t)$, where the intensity is maximum, with time in a reverse quench experiment from 119 °C to 114 °C. The circles denote the experimental values.

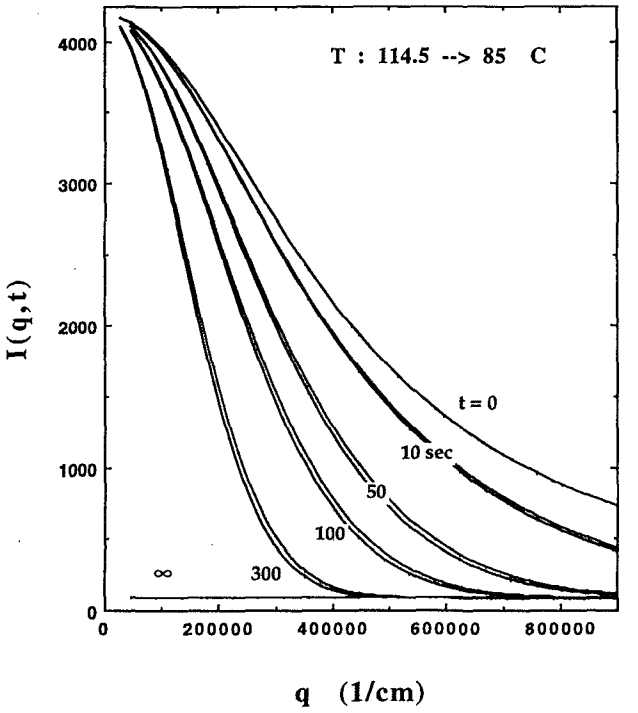

FIG. 7. Variation of intensity following a temperature drop from 114.5 °C to 85 °C, both within one-phase region. Upper curves: linear theory. Lower curves: nonlinear theory.

from Fig. 6 as $D_{in}(114\,°C)=3.82\times10^{-14}$ cm^2/s, which is about 1/2.8 of the value reported earlier[29] as $D_{in}(114\,°C)=10.9\times10^{-14}$ cm^2/s in an reverse quench experiment from 117 °C to 114 °C. The point we make with these comparisons is more to show that the experimentally observed asymptotic behavior is well explained with the theory, rather than proposing a method for an accurate evaluation of the interdiffusion coefficient from the intercept of the asymptote. However, even then the order of magnitude estimates based on Eq. (35) are consistent with the independent measurements.

Figures 4(a) and 4(b) show the variation the $Z(q,t)$ as function of wave number q at different dissolution times, and of time t at $q=25\,000$/cm, respectively. As stated earlier, $Z(q,t)$ represents the relative change in the relaxation frequency due to mode coupling, from $R(q)$ in the linear theory. The tendency towards a power law dependence in time for late times is noteworthy in Fig. 4(b). The values of $Z(q,t)$ seems to be small as compared to unity even for short times, indicating that the effect of mode coupling in reverse quench does not play an important role, at least with the numerical values used in the computations. In general, the effect of nonlinearities becomes more important when the final equilibrium state in the one-phase region is closer to the spinodal line, because than $Z_{eq}(q)$ becomes more significant as compared to unity [see Eq. (34b)].

A final comment is that the $t^{-0.5}$ dependence is predicted, and verified experimentally, only in the time intervals in which the thermal fluctuations, represented by $C(q)$ in Eq. (25), are not important (i.e., during dissolution stage). At later stages, there may not be a power law, or if there is, it may have a different exponent, because of the contribution of the second term in Eq. (25) which represent the effect of thermal fluctuations.

D. Step temperature changes in one-phase region

In this section we consider a step temperature drop from 114.5 °C to 85 °C, a temperature jump from 85 °C back to 114.5 °C. The required inputs are $\Lambda(114.5\,°C)=2.08\times10^{-10}$ cm^2/s, $\Lambda(85\,°C)=0.0316\times10^{-10}$ cm^2/s, $\chi(114.5\,°C)=0.91\,\chi_s$, and $\chi(85\,°C)=-3.48\chi_s$. The cutoff wave number q_{cut} was taken to be the inverse correlation length at the final temperature.

Figure 7 shows the variation of intensity following the temperature drop from 114.5 °C to 85 °C. The behavior of $I(q,t)$ does not display any interesting structure. The linear and nonlinear theories yield almost identical results with the values of the parameters used in the experiment. As expected, the mode coupling slightly increases the relaxation rates (the lower curves in Fig. 7). The effect of the mode coupling would be noticeable at least during the early relaxation times, if the initial interaction parameter $\chi(114.5\,°C)/\chi_s$ were closer to unity than 0.91.

Figure 8 depicts the variation of intensity following a temperature jump from 85 °C to 114.5 °C. Again, the linear and nonlinear theories give very similar results. However, the differences is expected to be appreciable when the final temperature approaches the spinodal temperature. The appearance of a peak as in spinodal decomposition, is somewhat surprising because there is no coarsening during the transition from an equilibrium state at a lower temperature to one at a higher temperature. The change in intensity

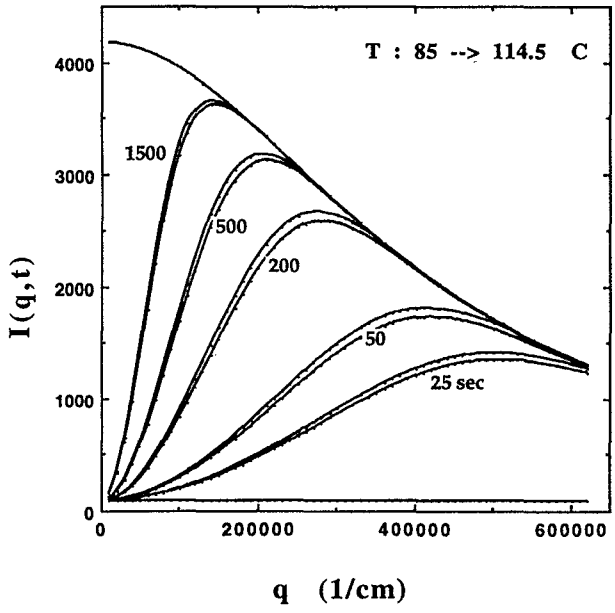

FIG. 8. Variation of intensity following a temperature jump from 85 °C to 114.5 °C, both within one-phase region. Upper curves: linear theory. Lower curves: nonlinear theory.

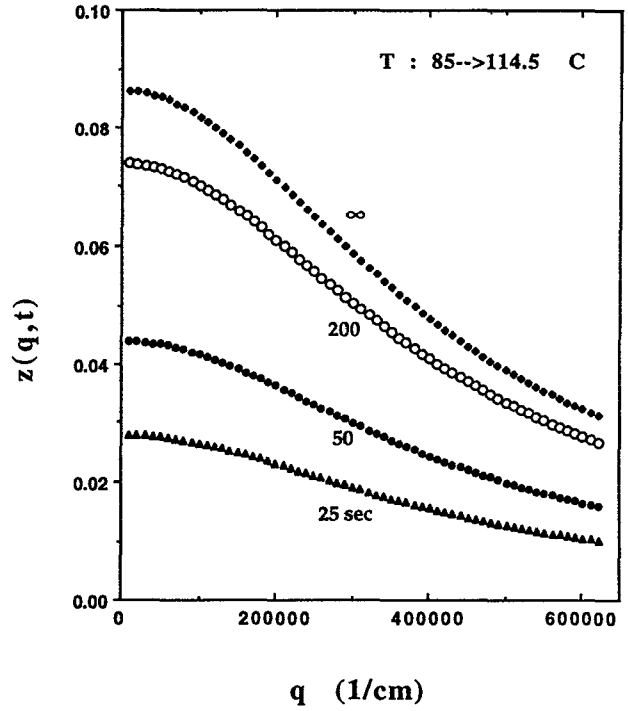

FIG. 10. Variation of $Z(q,t)$ in the expression of the instantaneous relaxation frequency $\Omega(q,t)=R(q)[1+Z(q,t)]$ with wave number and time in a temperature jump experiment within one-phase region (theoretical).

reflects both the increase in the magnitude of thermal fluctuation and in the correlation length. The latter increase in the size of statistically correlated domains may be interpreted as "coarsening" in statistical sense. The variation of the location of the peak as function of time is plotted in Fig. 9. It is interesting that $q_m(t)$ follows asymptotically a power law as $t^{-1/3}$, as in the case of spinodal decomposition.[34] This behavior can be shown analytically. Since there is no experimental data as yet to check these predictions, we shall not dwell on this point any longer.

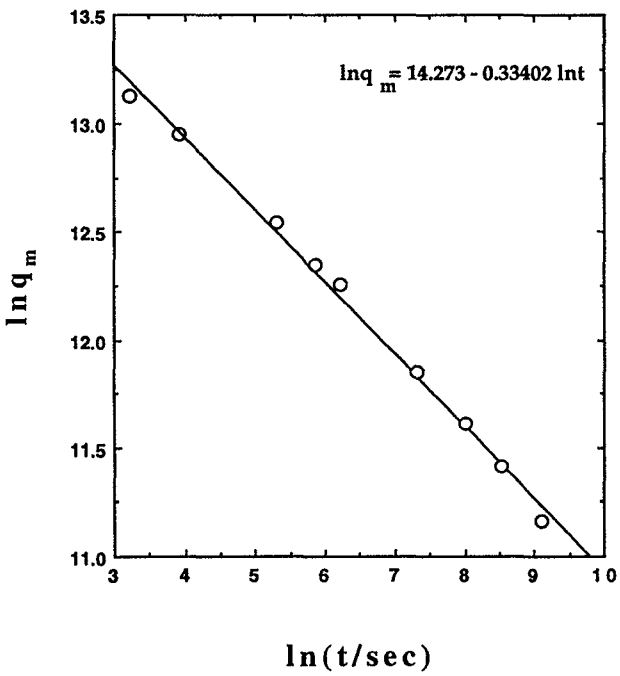

FIG. 9. Variation of the wave number $q_m(t)$, where the intensity is maximum, with time in a temperature jump experiment within one-phase region. The circles denote the theoretical values.

Figure 10 presents the variation of $Z(q,t)$ with wave number q for various times following the temperature jump from 85 °C to 114.5 °C. It is observed that the values of $Z(q,t)$ are small as compared to unity, indicating once more that the effect of mode coupling is not significant in this experiment, and the linear theory is sufficient to explain it. However, as the curves indicate, $Z(q,t)$ increases with time, and approaches to $Z_{eq}(q)$ as $t\to\infty$, at $T=114.5$ °C. The latter would increase very rapidly if the final temperature were closer to the spinodal temperature than 114.5 °C [see Eq. 34b], and the difference between the predictions of the linear and nonlinear theories would be increasingly more pronounced.

It follows from the above discussions that the simple theory used in this study is capable of reproducing most of the experimentally observed features of the scattering intensity during dissolution following a temperature drop from spinodal region into one-phase region. The predictions concerning the variation of the scattering intensity following step temperature changes within one-phase region, particularly following temperature jumps, remain to be verified experimentally.

ACKNOWLEDGMENTS

One of us (A.Z.A) thanks Alexander von Humboldt-Stiftung for making his stay at the Department of Physics

of the University of Konstanz, Konstanz, Germany, possible. He also thanks Professor R. Klein and his associates for their hospitality during his stay.

[1] For example, J. D. Gunton, M. Sam Miguel, and P. S. Sahni, in *Phase Transition and Critical Phenomena*, edited by C. Domb and J. L. Lebowitz (Academic, London, 1983), Vol. 8.
[2] J. W. Cahn and J. E. Hilliard, J. Chem. Phys. **28**, 258 (1958); *ibid.* **42**, 93 (1965).
[3] H. E. Cook, Acta Metall. **18**, 297 (1970).
[4] K. Binder, J. Chem. Phys. **79**, 6387 (1983).
[5] G. H. Fredrickson, J. Chem. Phys. **85**, 3556 (1986).
[6] P. G. de Gennes, J. Chem. Phys. **72**, 4756 (1980).
[7] P. Pincus, J. Chem. Phys. **75**, 1996 (1981).
[8] J. S. Langer, M. Bar-on, and H. D. Miller, Phys. Rev. A **11**, 1417 (1975).
[9] E. D. Siggia, Phys. Rev. A **20**, 595 (1979).
[10] H. Furukawa, Adv. Phys. **34**, 703 (1985).
[11] H. Furukawa, Physica A **123**, 497 (1984).
[12] H. Furukawa, Phys. Rev. Lett. **43**, 136 (1979).
[13] C. C. Han, M. Okada, Y. Muroga, F. L. McCrackin, B. J. Bauer, and Q. Tran-Cong, Polym. Eng. Sci. **26**, 3 (1986).
[14] M. Okada and C. C. Han, J. Chem. Phys. **85**, 5317 (1986).
[15] T. Nishi, T. T. Wang, and T. K. Kwei, Macromolecules **8**, 227 (1975).
[16] H. L. Snyder, P. Meaken, and S. Reich, Macromolecules **16**, 641 (1983).
[17] T. Hashimoto, J. Kumaki, and H. Kawai, Macromolecules **16**, 641 (1983).
[18] J. Kumaki and T. Hashimoto, Macromolecules **19**, 763 (1986).
[19] T. Izumitani and T. Hashimoto, J. Chem. Phys. **83**, 3694 (1985).
[20] T. Sato and C. C. Han, J. Chem. Phys. **88**, 2057 (1988).
[21] T. Hashimoto, M. Itakura, and H. Hasegawa, J. Chem. Phys. **85**, 6118 (1986).
[22] T. Hashimoto, M. Itakura, and N. Shimidzu, J. Chem. Phys. **85**, 6773 (1986).
[23] P. G. de Gennes, *Scaling Concepts in Polymer Physics* (Cornell University, Ithaca, 1979).
[24] M. Shibayama, H. Yang, R. S. Stein, and C. C. Han, Macromolecules **18**, 2179 (1985).
[25] A. Z. Akcasu and I. C. Sanchez, J. Chem. Phys. **88**, 7847 (1988).
[26] A. Z. Akcasu, Macromolecules **22**, 3682 (1989); A. Z. Akcasu and I. C. Sanchez, Mol. Cryst. Liq. Cryst. **180A**, 147 (1990).
[27] M. Lax, Rev. Mod. Phys. **32**, 25 (1960).
[28] J. S. Langer, *Nonlinear Phenomena at Phase Transitions and Instabilities* (Nato Advanced Study Institute, 1981, Geilo, Norway), edited by T. Riste (Plenum, New York, 1981).
[29] Y. Feng, C. C. Han, M. Takenaka, and T. Hashimoto, Polymer **33**, 2729 (1992).
[30] Certain commercial materials and equipment are identified in this paper in order to specify adequately the experimental procedure. In no case does such identification imply recommendation or endorsement by the National Institute of Standards and Technology, nor does it imply necessarily the best available for the purpose.
[31] N. j. Bauer, B. Hanly, and Y. Muroga, Polym. Commun. **30**, 19 (1989).
[32] M. He, Y. Liu, Y. Feng, M. Tiang, and C. C. Han, Macromolecules **24**, 464 (1991).
[33] These are not statistical segment lengths, but the step lengths that produce the measured radius of gyrations when used in $R_{g\alpha}=N_\alpha\sigma_\alpha^2/6$ with N_α being the actual number of monomers, which is of course different from the number of statistical segments.
[34] A. Z. Akcasu, B. Erman, and I. Bahar, *Proceeding of the Symposium on Thermodynamics of Polymers and Radiation Scattering* in Honor of Professor H. Benoit's 70th birthday (Die Makromolekulare Chemie) (in press).